

Article

Physical and Magnetic Properties of ThMn₁₂-Type Sm(Fe_{0.8}Co_{0.2})₁₀Si₂ Melt-Spun Ribbons

Hui-Dong Qian, Jung Tae Lim, Jong-Woo Kim, Yang Yang, Tian Hong Zhou, Han Kook Jeon, Jihoon Park *  and Chul-Jin Choi *

Powder Materials Division, Korea Institute of Materials Science, Changwon 51508, Korea; qhd771529249@gmail.com (H.-D.Q.); jungtae0401@kims.re.kr (J.T.L.); jwk@kims.re.kr (J.-W.K.); yolanda.yang.y@gmail.com (Y.Y.); zhouth@kims.re.kr (T.H.Z.); gksrnr0672@kims.re.kr (H.K.J.)
* Correspondence: jpark@kims.re.kr (J.P.); cjchoi@kims.re.kr (C.-J.C.)

Abstract: The magnetic properties of ThMn₁₂-type Fe-rich compounds were investigated by producing Sm(Fe_{0.8}Co_{0.2})₁₀Si₂ ribbons. The produced ribbons, with different conditions by varying the melt-spinning conditions, were characterized to investigate physical and magnetic properties. Weight fraction of ThMn₁₂-type phase decreased from 94.5 to 57.1 wt. % as the melt-spinning wheel speed increased from 6.5 to 39 m/s, and corresponding magnetizations and coercivities were substantially varied; the coercivity increased up to 0.175 T from 0.058 T by increasing the wheel speed from 6.5 to 26 m/s, and their magnetization also increased from 89.81 Am²/kg to 105.58 Am²/kg, even though the content of ThMn₁₂-type phase decreased. Morphologies of the ribbons were also observed to verify the melt-spinning effects on the surface conditions and grain sizes. It was found that the particle and grain sizes in the ribbons became smaller and striped patterns appeared as the wheel speed increased. The grain size decreased from about 1 μm to 250 nm by increasing the wheel speed from 6.5 to 39 m/s.



Citation: Qian, H.-D.; Lim, J.T.; Kim, J.-W.; Yang, Y.; Zhou, T.H.; Jeon, H.K.; Park, J.; Choi, C.-J. Physical and Magnetic Properties of ThMn₁₂-Type Sm(Fe_{0.8}Co_{0.2})₁₀Si₂ Melt-Spun Ribbons. *Metals* **2022**, *12*, 753. <https://doi.org/10.3390/met12050753>

Academic Editors: Imre Bakonyi and Jiro Kitagawa

Received: 8 March 2022

Accepted: 20 April 2022

Published: 28 April 2022

Publisher's Note: MDPI stays neutral with regard to jurisdictional claims in published maps and institutional affiliations.



Copyright: © 2022 by the authors. Licensee MDPI, Basel, Switzerland. This article is an open access article distributed under the terms and conditions of the Creative Commons Attribution (CC BY) license (<https://creativecommons.org/licenses/by/4.0/>).

Keywords: ThMn₁₂-type phase; Si substitution; magnetic properties; microstructure

1. Introduction

Rare-earth intermetallic compounds of R(Fe,M)₁₂ (R = rare earth elements, M = transition metals) with ThMn₁₂ structure have been known to be promising permanent magnetic materials since the 1980s [1]. Recently, increasing demand for raw rare earths motivated intensifying research on rare-earth-lean and rare-earth-free hard magnetic materials, which could “bridge” the performance gap between ferrite and Nd-Fe-B magnets [2]. R(Fe,M)₁₂ compounds with ThMn₁₂ structure show enough possibility to fill the gap as rare-earth-lean hard magnetic materials. In particular, Sm(Fe,M)₁₂ compounds show excellent intrinsic hard magnetic properties with saturation magnetization (*M_s*) of 1.78 T, anisotropy field (*H_a*) of 12 T, and Curie temperature (*T_c*) of 859 K, all of which are even higher than Nd-Fe-B compounds [3]. Besides the excellent magnetic properties, the lower cost of Sm than Nd in the Nd-Fe-B compounds also leads the Sm(Fe,M)₁₂ compounds to be superior to the most permanent magnets, including rare-earth permanent but also rare-earth-free magnets.

The crystal structure of ThMn₁₂ is originated from an unstable CaCu₅ structure with a 1:5 ratio of rare-earth elements (R) to 3*d* transition elements (T). By substituting more R and T elements into the CaCu₅ structure, the ThMn₁₂ structure is obtained. When the substituted R atoms are randomly positioned, the TbCu₇ structure is easily obtained with an R:T ratio ranging from 1:5 to 1:9 [4]. The ThMn₁₂ phase, however, is also unstable, and Fe atoms must be partially substituted with phase-stabilizing element(s), such as Ti, V, Cr, Mn, Mo, W, Al, and Si, which results in magnetization reduction [5–13]. The large transition metals, such as Ti, V, Mo, Ta, and W, occupy the 8*i* sites of R(Fe,M)₁₂, while the *sp* atoms, such as Al and Si, prefer the 8*f* sites [1,14,15]. The largest number of research

papers focus on Ti substitution as a phase-stabilizing element, since a small amount of Ti can effectively stabilize the ThMn_{12} -type phase, while higher concentrations of other elements, such as V, Cr, Mn, Mo, Al, and Si, are needed to stabilize the phase. Nevertheless, a number of research working on substituting such elements have also been performed in order to enhance magnetic properties including coercivity (H_c). Among the above elements, Si is one of the cheapest elements that can possibly enhance the H_c by increasing single domain size or segregating at the grain boundary phase.

However, the Si substituted R(Fe,M)_{12} compounds have not been widely investigated, even though preceding research verifies that R(Fe,Si)_{12} compounds could exhibit outstanding magnetic properties [16,17]. Due to the high formation temperature of the ThMn_{12} structure, it is a challenging task to successfully obtain nano-sized grains for a high H_c [18]. Previously, Qian et al. substituted both Ti and Si in R(Fe,M)_{12} to obtain ThMn_{12} -type phase with a higher stability than Ti-only substituted structure, but it was found that the Ti and Si substituted R(Fe,Si)_{12} exhibits degraded H_c [19]. Finding a way to stabilize the nano-structure during the solidification and high-temperature treatment is essential to develop Si-substituted R(Fe,M)_{12} compounds.

In order to extend the study of melt-spun ternary alloys R(Fe,Si) , we report, in this paper, our results concerning the influences of melt-spinning conditions on weight fractions of crystallized phases and their lattice parameters, magnetic properties, and morphologies. The wheel speeds during the melt-spinning processes decisively affect the ribbon conditions. The phase stabilities of the melt-spun ribbons is also discussed to clarify the effect of Si substitution in R(Fe,M)_{12} compounds.

2. Experiment

Ingots with nominal compositions, $\text{Sm(Fe}_{0.8}\text{Co}_{0.2})_{10}\text{Si}_2$, were prepared by arc-melting high-purity Sm (99.9%), Fe (99.95%), Co (99.95%), and Si (99.9%) pieces under an Ar atmosphere. An excess of Sm of 30 at. % was included in the alloys to compensate for the Sm evaporation loss and obtain a high-purity ThMn_{12} -type phase. The ingots were melted in an Ar environment in quartz nozzles and ejected through a 0.4 mm orifice using pressurized Ar gas onto a copper wheel rotating at a velocity of 6.5–39 m/s.

The crystalline structure and phase purities of the products were characterized using X-ray diffraction (XRD) with $\text{Cu-K}\alpha$ ($\lambda = 1.5406 \text{ \AA}$) radiation; the measured XRD patterns were analyzed using the Rietveld refinement method with the FullProf program (version 7.20). The morphologies of the ribbons were examined using a Field emission scanning electron microscope (FE-SEM, JSM-7001F, JEOL, Akishima, Tokyo, Japan). The high-resolution morphologies of the bulks were observed using scanning transmission electron microscopy (STEM, JEM 2100F, JEOL, Akishima, Tokyo, Japan). The TEM specimens were prepared using a focused ion beam. Magnetic properties of the ribbon and bulk samples were measured using a vibrating sample magnetometer (VSM, MicroSense LLC, Lowell, MA, USA).

3. Results and Discussion

The XRD patterns of manually ground $\text{Sm(Fe}_{0.8}\text{Co}_{0.2})_{10}\text{Si}_2$ ribbons with different wheel speeds are shown in Figure 1. Phase identities and their weight fractions were analyzed using the Rietveld refinement method with the FullProf program. The four ground ribbons were mainly found to be mixtures of a tetragonal structure with a space group of $I4/mmm$ and a hexagonal structure with a space group of $P6/mmm$, which indicate ThMn_{12} -type and TbCu_7 -type phases, respectively. A small amount, less than 1 wt. %, of α -Fe phase was observed in the ribbons with the wheel speed of 6.5 m/s. The weight fraction of the ThMn_{12} -type phase decreased from 94.5 to 57.1 wt. % with the increasing wheel speed, while the TbCu_7 -type phase simultaneously increased from 4.7 to 42.9 wt. % as listed in Table 1. Due to the high quenching rate by the melt spinning, an amorphous phase could be formed in the ribbons, where its fraction certainly increases with the increasing quenching rate [20]. It is noted that the fraction of the amorphous phase is not included in Table 1. The decreasing peak intensities and their broadening widths in Figure 1, with the increasing

wheel speed, correspond to the decreasing grain sizes of the crystallized ThMn₁₂-type and TbCu₇-type phases. Lattice parameters *a* and *c* of ThMn₁₂-type and TbCu₇-type phases in the samples with different wheel speeds are also listed in Table 1. The increase in wheel speed from 6.5 to 39 m/s led to the change in lattice parameters. The parameters *a* and *c* of ThMn₁₂-type and TbCu₇-type change irregularly when the wheel speed increase from 6.5 to 39 m/s. However, for the 26 m/s melt-spun ribbons, the *c/a* of ThMn₁₂-type gets the highest point of 0.5571 while the *c/a* of TbCu₇-type gets the lowest point of 0.8546. The calculated average atomic volumes of ThMn₁₂-type and TbCu₇-type increased linearly due to increased cell volumes when the solidification rate increased.

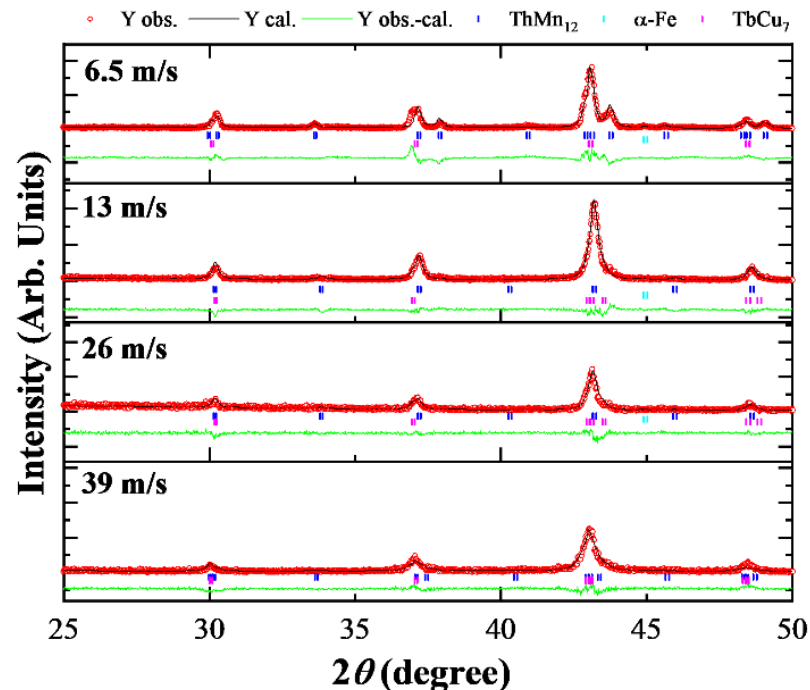


Figure 1. Refined X-ray diffraction patterns of the Sm(Fe_{0.8}Co_{0.2})₁₀Si₂ melt-spun ribbons with different wheel speeds.

Table 1. Lattice parameters *a* and *c*, *c/a*, and average atomic volumes (*V*, Å³) of ThMn₁₂-type and TbCu₇-type phases and weight fraction (wt. %) of ThMn₁₂, TbCu₇, and α-Fe phases in the Sm(Fe_{0.8}Co_{0.2})₁₀Si₂ melt-spun ribbons with different wheel speeds. The values of lattice parameters have a confidence interval of ±0.005 according to the deviation from measurement and refinement.

Wheel Speed (m/s)	ThMn ₁₂				TbCu ₇				ThMn ₁₂ (wt. %)	TbCu ₇ (wt. %)	α-Fe (wt. %)
	<i>a</i> (Å)	<i>c</i> (Å)	<i>c/a</i>	<i>V</i> (Å ³)	<i>a</i> (Å)	<i>c</i> (Å)	<i>c/a</i>	<i>V</i> (Å ³)			
6.5	8.432	4.748	0.5631	12.98	4.854	4.183	0.8618	36.54	94.5	4.7	0.8
13	8.378	4.820	0.5753	13.01	4.847	4.148	0.8558	36.62	84.5	14.7	0.8
26	8.384	4.838	0.5771	13.08	4.863	4.156	0.8546	36.81	70.2	29.8	0
39	8.424	4.804	0.5703	13.11	4.850	4.212	0.8685	36.90	57.1	42.9	0

The magnetic properties of the Sm(Fe_{0.8}Co_{0.2})₁₀Si₂ ribbons with different quenching rates by different wheel speeds were also investigated, as shown in Figure 2. Magnetic hysteresis loops of the four samples were measured at room temperature with a maximum magnetic field of 2.5 T. The detailed magnetic properties, including magnetization at 2.5 T (*M*_{2.5T}), remanent magnetization (*M*_r), *H*_c, and *T*_c, are listed in Table 2. The increasing wheel speed resulted in decreasing grain size, as can be seen in Figure 1, which resulted in the enhanced *H*_c from 0.058 to 0.175 T until the speed reached 26 m/s, even though the weight fraction of the ThMn₁₂-type phase decreased from 94.5 to 70.2 wt. %, as listed in Table 1. Tomoko Kuno et al. also reported that a mixture phase of 1:9 and 1:12 could have

higher H_c than pure 1:9 or 1:12 [21]. On the other hand, the H_c decreased to 0.137 T due to the low weight fraction of ThMn₁₂-type phase of 57.1 wt. %, high content of TbCu₇-type of 42.9 wt. %, and the existence of the amorphous phase according to the increased broadness of the observed XRD peak. The $M_{2.5T}$ of the ribbon with the highest weight fraction of the ThMn₁₂-type phase was 89.81 Am²/kg, which increased with the increasing wheel speed to 111.09 and 105.58 Am²/kg for the wheel speeds of 13 and 26 m/s, respectively. Like the H_c , the $M_{2.5T}$ also dramatically decreased to 70.29 Am²/kg when the wheel speed was 39 m/s due to the low weight fraction of the ThMn₁₂-type phase. The corresponding M_r were also enhanced from 29.63 to 56.09 Am²/kg due to the increased $M_{2.5T}$ and H_c up to the wheel speed of 26 m/s and then decreased to 29.63 Am²/kg at the higher wheel speed. It is noted that the deterioration of magnetization and H_c were also attributed to the highly possible existence of the amorphous phase in the ribbons.

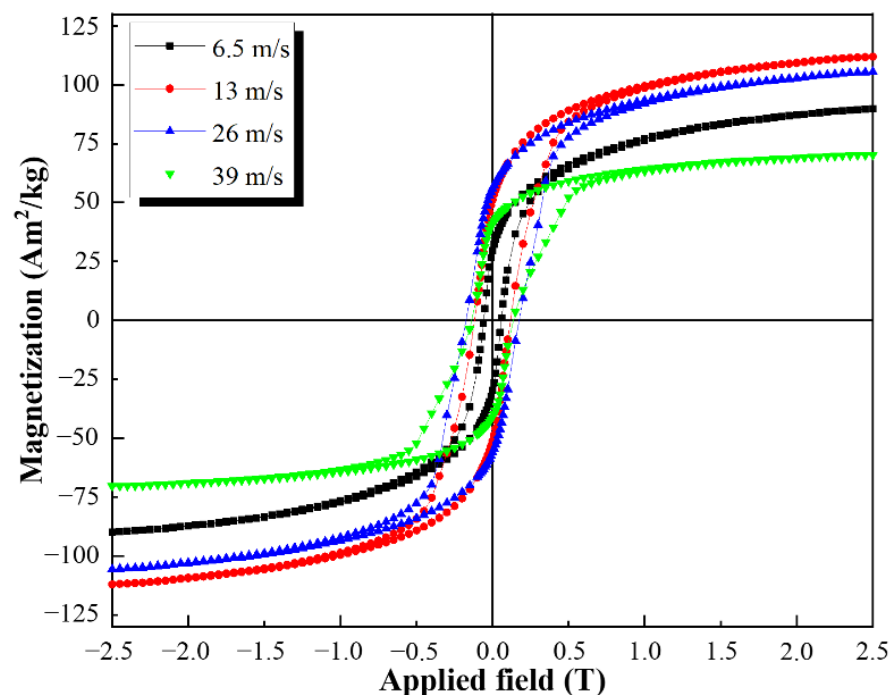


Figure 2. Magnetic hysteresis loops of the Sm(Fe_{0.8}Co_{0.2})₁₀Si₂ ribbons with different wheel speeds.

Table 2. Magnetization at 2.5 T ($M_{2.5T}$), remanent magnetization (M_r), coercivity (H_c), and Curie temperature (T_c) of the Sm(Fe_{0.8}Co_{0.2})₁₀Si₂ ribbons with different wheel speeds.

Wheel Speed (m/s)	$M_{2.5T}$ (Am ² /kg)	M_r (Am ² /kg)	H_c (T)	T_{c1} (K)	T_{c2} (K)
6.5	89.81	29.63	0.058	653	733
13	111.09	51.20	0.118	694	726
26	105.58	56.09	0.175	684	719
39	70.29	29.63	0.137	689	718

Normalized temperature dependences of magnetizations from 300 to 1000 K under an applied field of 0.02 T for the four ribbon samples were measured, as shown in Figure 3a. The T_c were obtained by differentiating the curves in Figure 3a and finding maximum curvatures points, as shown in Figure 3b. The obtained T_c are listed in Table 2. All of the dM/dT curves in Figure 3b show two peaks, i.e., T_{c1} and T_{c2} , which means that two magnetic phases coexist in the ribbons according to the results presented by Saito et al. on the microstructure of TbCu₇ and ThMn₁₂ melt-spun ribbons [22], first at a lower temperature, after which the ThMn₁₂ is crystallized at a higher temperature during the heat treatment process. Furthermore, the T_c of the TbCu₇ is also lower than the ThMn₁₂.

Therefore, we could identify T_{c1} as belonging to the TbCu_7 -type phase and T_{c2} as belonging to the ThMn_{12} . The varying T_{c1} and T_{c2} in Figure 3b are attributed to the existing crystalline phases, such as the TbCu_7 and ThMn_{12} . The T_{c1} increased from 653 to 694 K according to the increasing wheel speed from 6.5 to 13 m/s. The T_{c2} decreased from 733 to 718 K when the wheel speed increased from 6.5 to 39 m/s. It is noted that the T_c for all the samples are significantly higher than the T_c of 590 K for the $\text{Nd}_2\text{Fe}_{14}\text{B}$ magnet [23,24]. In conclusion, the sample consisted of 70.2 wt. % of ThMn_{12} -type phase and 29.8 wt. % of TbCu_7 -type phase, which was melt spun at the wheel speed of 26 m/s, exhibiting the highest M_r and H_c among the fabricated samples.

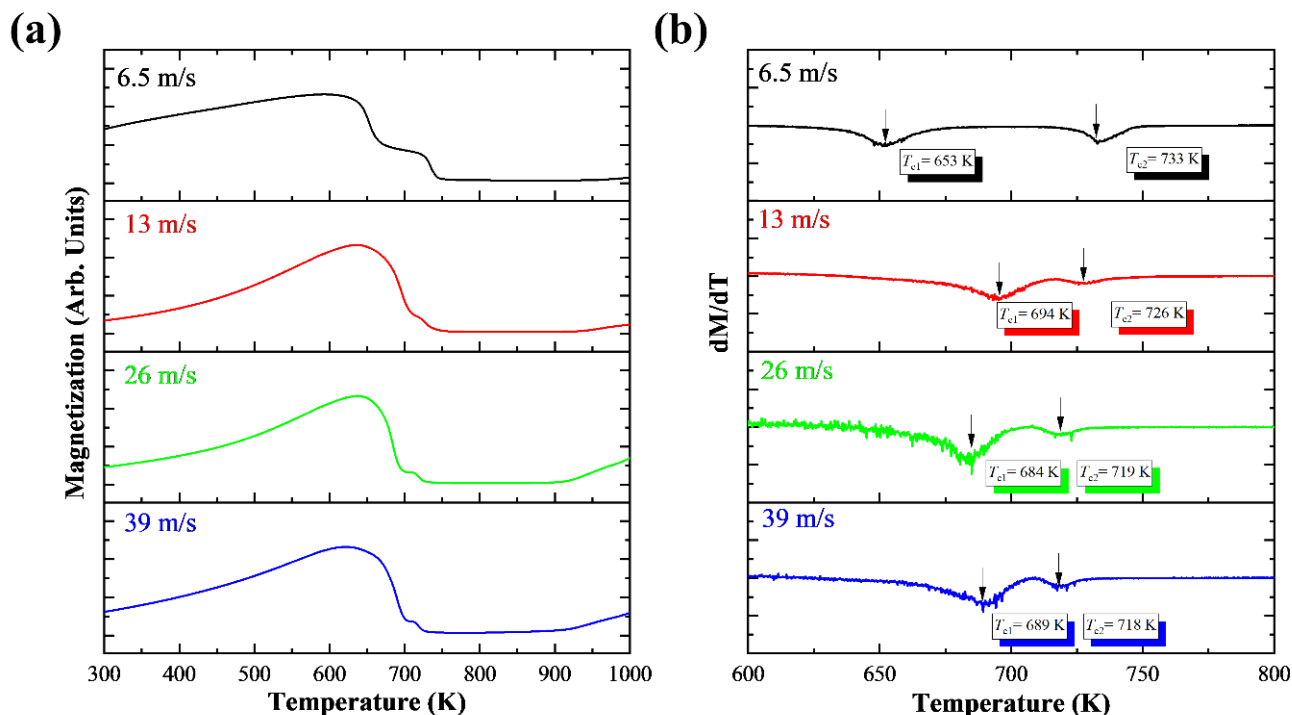


Figure 3. Temperature dependences of (a) normalized magnetizations and (b) temperature derivative of magnetization (dM/dT) curves of the $\text{Sm}(\text{Fe}_{0.8}\text{Co}_{0.2})_{10}\text{Si}_2$ ribbons with different wheel speeds under an applied magnetic field of 0.02 T.

Microstructures of the melt-spun ribbons with different wheel speeds were observed. SEM and back-scattered electrons (BSE) images of the four samples in Figure 4 show clear differences in the microstructure. The sample melt spun at the wheel speed of 6.5 m/s consists of random-shaped particles (marked in red circles) of 20–35 μm in diameter, as shown in Figure 4a,e. The particles in the sample with the wheel speed of 13 m/s in Figure 4b,f are unclearly shaped but are certainly aligned based on the striped patterns on the surface. During the melt-spinning process, the solidification occurs along the rolling wheel direction due to its high-speed wheel, which directly contacts the ejected molten ingots. Therefore, the striped patterns and particles become conspicuous and elongated with the increasing wheel speed. The particle size of the sample melt spun at the wheel speed of 26 m/s range from 4.5 to 10 μm , and overall strips are along the wheel direction as shown in Figure 4c,g. The strips and particle size for the sample melt spun at the wheel speed of 39 m/s are more obviously elongated, as shown in Figure 4d,h. The particle size of the columnar-like particles in Figure 4d,h are 4–9 μm in the longitudinal direction and 2–3 μm in the transverse direction.

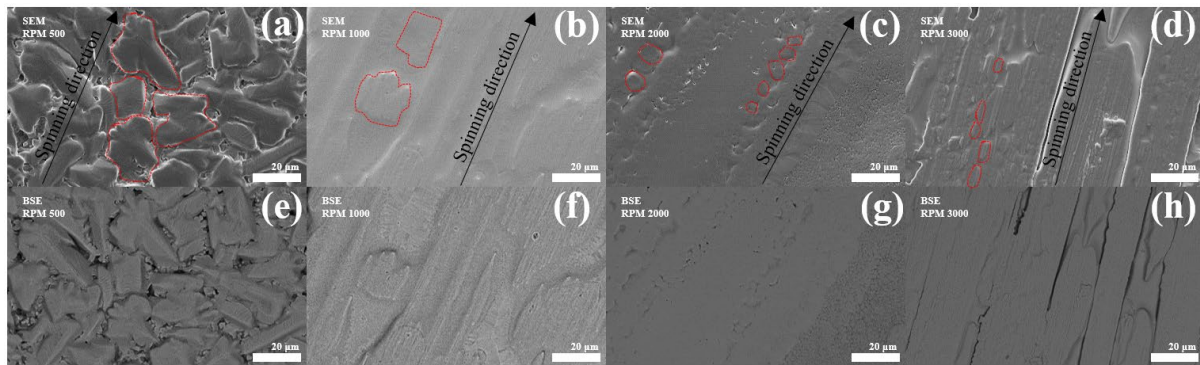


Figure 4. SEM and BSE images of the $\text{Sm}(\text{Fe}_{0.8}\text{Co}_{0.2})_{10}\text{Si}_2$ ribbons with the wheel speeds of (a,e) 6.5, (b,f) 13, (c,g) 26, and (d,h) 39 m/s, respectively.

Magnetic properties, especially H_c , are strongly related to grain sizes of magnetic materials. Grain boundaries and impurities act as pinning centers for the domain walls by strongly inhibiting their motion, and thus reducing the efficiency of this reversal mechanism. However, if the grain size itself is not close to the single domain size, the grain boundaries and pinning centers cannot effectively play a role to increase the H_c . In order to increase the H_c , it is worth decreasing grain size to near the single domain size. Figure 5a is a high-angle annular dark-field (HAADF) image of the sample with the wheel speed of 6.5 m/s. The indicated grains with red and blue colors were analyzed to be ThMn_{12} -type and TbCu_7 -type phases, respectively, using energy-dispersive X-ray spectroscopy (EDS). Figure 5b–e are high-resolution transmission electron microscopy (HRTEM) images of the samples with the wheel speeds of 6.5, 13, 26, and 39 m/s, respectively. According to the figures, the average grain size significantly decreased from about 1 μm to 250 nm, and the grain boundaries become unclear due to the increasing content of the amorphous phase by increasing the wheel speed from 6.5 to 39 m/s.

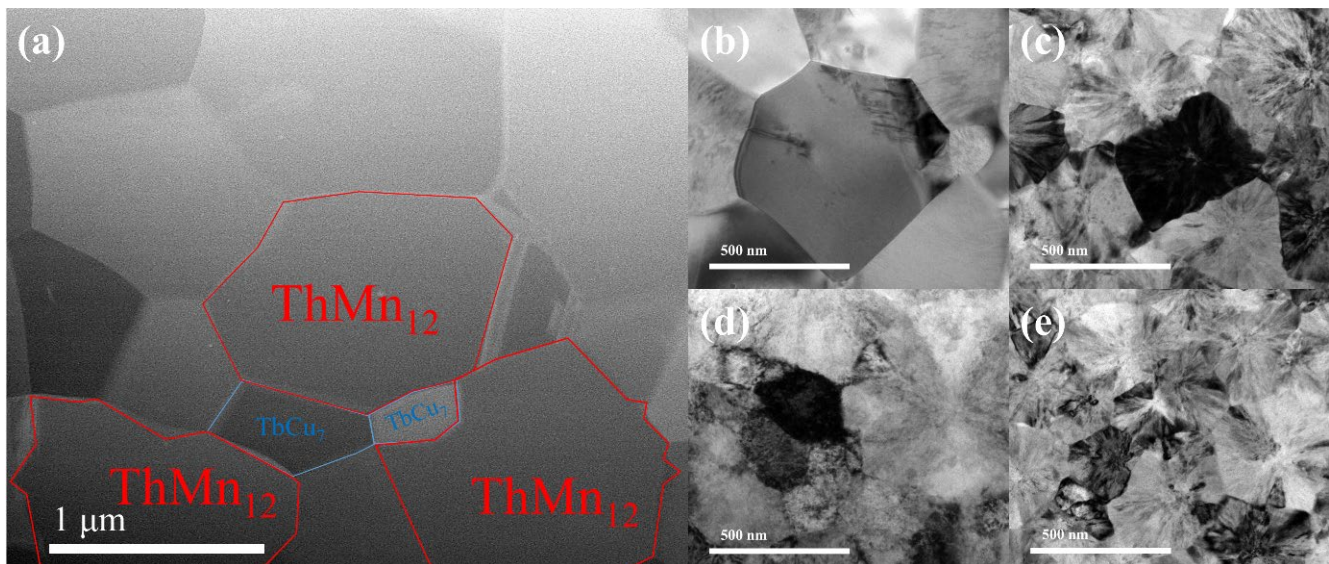


Figure 5. (a) HAADF image of the sample with the wheel speed of 6.5 m/s and HRTEM images of the $\text{Sm}(\text{Fe}_{0.8}\text{Co}_{0.2})_{10}\text{Si}_2$ ribbons with the wheel speeds of (b) 6.5, (c) 13, (d) 26 m/s, and (e) 39 m/s.

4. Conclusions

We successfully fabricated $\text{Sm}(\text{Fe}_{0.8}\text{Co}_{0.2})_{10}\text{Si}_2$ ribbons with hard magnetic ThMn_{12} -type and TbCu_7 -type phases. It was found that the increasing wheel speed results in the decreasing content of ThMn_{12} -type phase, while it increases the TbCu_7 -type phase. The highest coercivity among the samples with different wheel speeds appeared not in the

case that the weight fraction of ThMn₁₂-type is the highest but in the case that the weight fraction of ThMn₁₂-type phase is 70.2% and that of TbCu₇-type is 29.8%. Grain size of the ribbons decreased with the increasing wheel speed, therefore decreasing the grain size from about 1 μm to 250 nm. A precise control of phase transformation and prevention of grain growth in the Si-substituted Fe-rich compounds are key technologies to further enhance magnetic properties in the future.

Author Contributions: Conceptualization, H.-D.Q. and J.P.; methodology, H.-D.Q.; software, J.T.L.; validation, H.-D.Q., J.-W.K. and Y.Y.; formal analysis, H.-D.Q.; investigation, H.-D.Q.; resources, C.-J.C.; data curation, Y.Y., T.H.Z. and H.K.J.; writing—original draft preparation, H.-D.Q.; writing—review and editing, J.P.; visualization, J.P.; supervision, C.-J.C.; project administration, C.-J.C.; funding acquisition, C.-J.C. All authors have read and agreed to the published version of the manuscript.

Funding: This work was partially supported by the Future Materials Discovery Program through the National Research Foundation of Korea (NRF), funded by the Ministry of Science and ICT (2016M3D1A1027835), and by the Korea Institute of Energy Technology Evaluation and Planning (KETEP) grant funded by the Korean Ministry of Trade, Industry, and Energy (MOTIE) (20192010106850, Development of magnetic materials for IE4 class motor).

Conflicts of Interest: The authors declare no conflict of interest.

References

- Hadjipanayis, G.C.; Gabay, A.M.; Schönhöbel, A.M.; Martín-Cid, A.; Barandiaran, J.M.; Niarchos, D. ThMn₁₂-type alloys for permanent magnets. *Engineering* **2020**, *6*, 141–147. [\[CrossRef\]](#)
- Gabay, A.M.; Hadjipanayis, G.C. ThMn₁₂-type structure and uniaxial magnetic anisotropy in ZrFe₁₀Si₂ and Zr_{1-x}Ce_xFe₁₀Si₂ alloys. *J. Alloys Compd.* **2016**, *657*, 133–137. [\[CrossRef\]](#)
- Hirayama, Y.; Takahashi, Y.K.; Hirosawa, S.; Hono, K. Intrinsic hard magnetic properties of Sm(Fe_{1-x}Co_x)₁₂ compound with the ThMn₁₂ structure. *Scr. Mater.* **2017**, *138*, 62–65. [\[CrossRef\]](#)
- Takahashi, Y.K.; Sepehri-Amin, H.; Ohkubo, T. Recent advances in SmFe₁₂-based permanent magnets. *Sci. Technol. Adv. Mater.* **2021**, *22*, 449–460. [\[CrossRef\]](#)
- Ogawa, D.; Xu, X.D.; Takahashi, Y.K.; Ohkubo, T.; Hirosawa, S.; Hono, K. Emergence of coercivity in Sm(Fe_{0.8}Co_{0.2})₁₂ thin films via eutectic alloy grain boundary infiltration. *Scr. Mater.* **2019**, *164*, 140–144. [\[CrossRef\]](#)
- Fuji, H.; Sun, H. Interstitially modified intermetallics of rare earth and 3D elements. In *Handbook of Magnetic Materials*; Springer Science+Business Media: New York, NY, USA, 1995; Volume 9, pp. 303–404. [\[CrossRef\]](#)
- Tozman, P.; Sepehri-Amin, H.; Takahashi, Y.K.; Hirosawa, S.; Hono, K. Intrinsic magnetic properties of Sm(Fe_{1-x}Co_x)₁₁Ti and Zr-substituted Sm_{1-y}Zr(Fe_{0.8}Co_{0.2})_{11.5}Ti_{0.5} compounds with ThMn₁₂ structure toward the development of permanent magnets. *Acta Mater.* **2018**, *153*, 354–363. [\[CrossRef\]](#)
- Tozman, P.; Sepehri-Amin, H.; Zhang, L.T.; Wang, J.; Xu, X.D.; Hono, K. An alternative approach to the measurement of anisotropy field—Single grain extraction. *J. Magn. Magn. Mater.* **2020**, *494*, 165747. [\[CrossRef\]](#)
- Kuno, T.; Suzuki, S.; Urushibata, K.; Kobayashi, K.; Sakuma, N.; Yano, M.; Kato, A.; Manabe, A. (Sm,Zr)(Fe,Co)_{11.0-11.5}Ti_{1.0-0.5} compounds as new permanent magnet materials. *AIP Adv.* **2016**, *6*, 025221. [\[CrossRef\]](#)
- Coehoorn, R. Electronic structure and magnetism of transition-metal-stabilized YFe_{12-x}M_x intermetallic compounds. *Phys. Rev. B.* **1990**, *41*, 11790. [\[CrossRef\]](#)
- Li, H.S.; Coey, J.M.D. Magnetic properties of ternary rare-earth transition-metal compounds handbook of magnetic materials. In *Handbook of Magnetic Materials*; Springer Science+Business Media: New York, NY, USA, 1991; Volume 6, pp. 1–83. [\[CrossRef\]](#)
- Fukazawa, T.; Akai, H.; Hirayama, Y.; Miyake, T. First-principles study of intersite magnetic couplings and curie temperature in RFe_{12-x}Cr_x (R=Y, Nd, Sm). *J. Phys. Soc. Jpn.* **2018**, *87*, 044706. [\[CrossRef\]](#)
- Chen, N.X.; Hao, S.Q.; Wu, Y.; Shen, J. Phase stability and a site preference of Sm(Fe, T)₁₂. *J. Magn. Magn. Mater.* **2001**, *233*, 169–180. [\[CrossRef\]](#)
- Buschow, K.H.J. Permanent magnet materials based on tetragonal rare earth compounds of the type RFe_{12-x}M_x. *J. Magn. Magn. Mater.* **1991**, *100*, 79–89. [\[CrossRef\]](#)
- Bacmann, M.; Baudalet, C.; Fruchart, D.; Gignoux, D.; Hlil, E.K.; Krill, G. Exchange interactions and magneto-crystalline anisotropy in RFe_{12-x}M_x and parent interstitial compounds. *J. Alloys Compd.* **2004**, *383*, 166–172. [\[CrossRef\]](#)
- Gabay, A.M.; Schegoleva, N.N.; Belozarov, E.V. The structure and hard magnetic properties of rapid quenched (Sm,Zr)₁(Fe,Si)₁₂ alloys. *Phys. Met. Metallogr.* **2002**, *94*, 252–257.
- Ding, J.; Rosenberg, M. Magnetic properties of melt spun and crystallized SmFe₁₀M₂. *J. Magn. Magn. Mater.* **1990**, *83*, 257–258. [\[CrossRef\]](#)
- Gabay, A.M.; Hadjipanayis, G.C. Mechanochemical synthesis of magnetically hard anisotropic RFe₁₀Si₂ powders with R representing combinations of Sm, Ce, and Zr. *J. Magn. Magn. Mater.* **2017**, *422*, 43–48. [\[CrossRef\]](#)

19. Qian, H.D.; Lim, J.T.; Kim, J.W.; Yang, Y.; Zhou, T.H.; An, S.Y.; Jeon, H.K.; Cho, K.M.; Park, J.H.; Choi, C.J. Crystallization and magnetic properties of ThMn₁₂-type Sm-Fe-Co-Ti-Si based magnetic materials. *J. Mater. Res. Technol.* **2022**, *16*, 1458–1465. [[CrossRef](#)]
20. Qian, H.D.; Lim, J.T.; Kim, J.W.; Yang, Y.; Cho, K.M.; Park, J.H.; Choi, C.J. Phase transformation and magnetic properties of fully dense Sm(Fe_{0.8}Co_{0.2})₁₁Ti bulk magnets. *Scr. Mater.* **2021**, *193*, 17–21. [[CrossRef](#)]
21. Kuno, T.; Yamamoto, T.; Urushibata, K.; Kobayashi, K.; Sugimoto, S. Preparation of High-Coercivity Magnetic Powder via Heat Treatment of a Rapidly Quenched Amorphous Starting Compound with a ThMn₁₂ Structure. *Mater. Trans.* **2020**, *61*, 657–662. [[CrossRef](#)]
22. Saito, T.; Miyoshi, H.; Nishio-Hamane, D. Magnetic properties of Sm–Fe–Ti nanocomposite magnets with a ThMn₁₂ structure. *J. Alloys Compd.* **2012**, *519*, 144–148. [[CrossRef](#)]
23. Grössinger, R.; Krewenka, R.; Sun, X.K.; Eibler, R.; Kirchmayr, H.R.; Buschow, K.H.J. Magnetic phase transitions and magnetic anisotropy in Nd₂Fe_{14–x}Co_xB compounds. *J. Less Comm. Met.* **1986**, *124*, 165–172. [[CrossRef](#)]
24. Hirosawa, S.; Matsuura, Y.; Yamamoto, H.; Fujiura, S.; Sagawa, M.; Yamauchi, H. Magnetization and magnetic anisotropy of R₂Fe₁₄B measured on single crystals. *J. Appl. Phys.* **1986**, *59*, 873. [[CrossRef](#)]